Indonesian Journal of Aerospace Vol. 32 No. 2 December 2025 : pp 77–94 (Syamsudin et al.)
DOI: 10.55981/ijoa.2025.7078
https://ejournal.brin.go.id/ijoa/

On the Use of the Cohesive Zone Model in Validating Mixed-Mode Bending Apparatus Design

Muhammad Daffa Adhitama[1], M G Suada[2], Hendri Syamsudin[2]

[1]Post Graduate Study, Aeronautics and Astronautics Department
[2]Solid Mechanics and Lightweight Structure Research Group,
Faculty of Mechanical and Aerospace Engineering, Institut Teknologi Bandung,
Jalan Ganesa No. 10, Bandung 40132, Indonesia
e-mail: hendri.syamsudin@itb.ac.id

Received: 04-09-2024. Accepted: 30-04-2025. Published: 12-02-2026

Abstract

Understanding the strength of adhesive materials has been increasingly relevant due to their expanding use in many industries. The importance of understanding its mixed-mode behavior also increases since realistic loading cases rarely involve pure mode I and pure mode II loads. The mixed-mode bending (MMB) test, standardized by ASTM D6671, is a particularly intriguing test that could be used to map adhesive strength in a whole range of mixed-mode ratios, only by using a single specimen design. An MMB apparatus design has been developed based on guidelines provided by ASTM D6671 to test aluminum adherends with modifications that conform to local manufacturing capabilities and material availability. This design was then numerically inspected using the Cohesive Zone Model (CZM) and Benzeggagh-Kenane (B-K) model to check its validity and understand its work range. Mesh convergence test, adherend stiffness variation, and adhesive strength variation were conducted in ABAQUS. Results show satisfactory stability and validity of the design to test aluminum adherends.

Keywords: Mixed-mode bending, Mixed-mode ratio, Aluminum adherends, Cohesive zone model (czm), b-k model.

1. Introduction

Adhesive materials have become increasingly relevant in various industries as the choice material to bond structures due to their advantages compared to conventional mechanical joints (Borges, et al., 2023). Adhesive joints remove the need to damage material during joining (which is inevitable in mechanical joints such as rivets and bolts) and enable joining dissimilar materials with minimum risk of galvanic corrosion (Marques, et al., 2020). Adhesive joints have been widely used to bond layers of composite laminates and bond dissimilar joints such as bimetal joints or composite-metal joints (Marques, et al., 2020).

Understanding the material characteristics of adhesive materials is thus paramount in perfecting the implementation of adhesive bonding, ensuring reliable bonds that hold the benefits mentioned above, and having adequate strength to maintain structural integrity. Thus, multiple standard testing methods have been implemented to characterize the strength of adhesive materials such as Double Cantilevered Beam (DCB) test (ASTM D5528), Single Lap Joint (SLJ) test (ASTM 3163), End-Notched Flexure (ENF) test (ASTM D7905), and Mixed-Mode Bending (MMB) test (ASTM D6671). These tests aim to measure the strength of adhesive materials under different loading modes, including mode I loading (DCB), mode II loading (SLJ, ENF), and mixed-mode loading (MMB).

The MMB test is particularly interesting due to the existing interaction of mode I and mode II strength, with each material having its own interaction and thus having unique mixed-mode behavior. The MMB test can be used to test adhesively bonded joint specimens under different

mixed-mode loadings. Therefore, the entire mixed-mode behaviour of an adhesive material can be obtained through multiple tests.

The MMB test is done by simultaneously applying two loads to a specimen, similar to the DCB test, using a lever with a variable loading point. The setup of an MMB test, as originally designed by Reeder (Reeder & Crews, 1988) (Reeder & Crews, Jr., 1991) (Reeder, 2003), is shown in Figure 1-1.

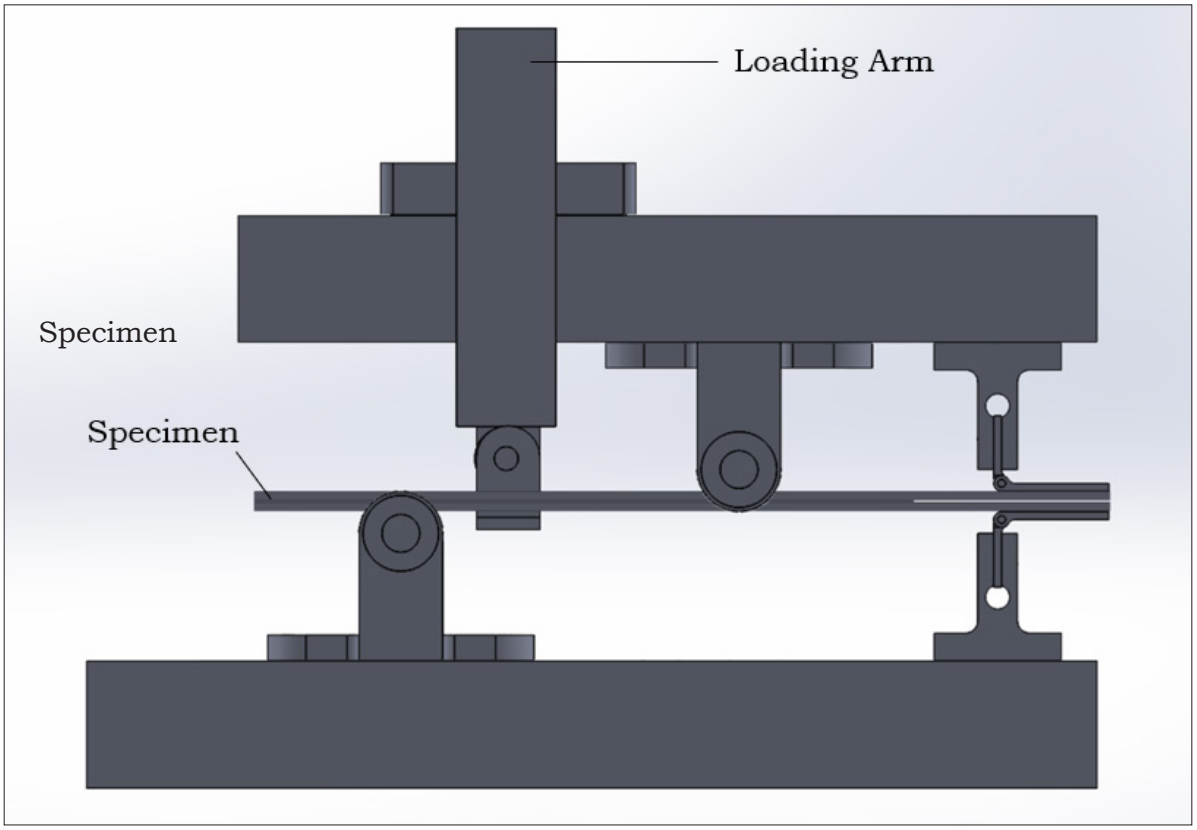

Figure 1-1: MMB Test Setup.

The lever gives an upward load at the specimen tip and a downward load at the middle of the specimen. The loading at the tip of the specimen is given using hinges and tabs, while the loading at the middle of the specimen is given using a roller. This load can be described as a combination of primary mode I and mode II loading, as shown in Figure 1-2. The loading point can be varied to exert a load with a different mixed-mode ratio. The base holds the specimen in place by the tabs connected to a pin at the tip of the specimen and a roller at the other tip.

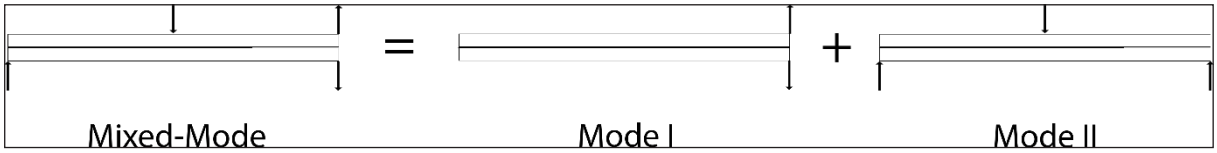

Figure 1-2: Mixed-Mode Loading as A Combination of Pure Mode I Loading and Pure Mode II Loading (Reeder, 2003).

The experiment is done by giving the load described above and measuring the force and displacement at the loading point. Then, from the force-displacement data, the adhesive material's mode I and mode II fracture toughness can be determined (American Society for

Testing and Materials, 2006). Due to the nature of the loading setup, the MMB test has many nonlinearities that significantly influence the results. Reeder (Reeder, 2003) addressed these nonlinearities and pointed out four significant root causes: the crack tip opening, the lever rotation, the specimen rotation, and the loading rotation. To minimize these nonlinearities, a modification was added to the MMB setup, such as the use of a saddle for a more consistent loading direction (Reeder & Crews, Jr., 1991). Several criteria were also derived to avoid huge nonlinearities (Reeder, 2003).

ASTM D6671 (American Society for Testing and Materials, 2006) recommends using the MMB test to evaluate the adhesive bonding of layers in a unidirectional composite material. However, the test can also be used to test other materials bonded with adhesives. Aluminum remains the most used metal in aerospace structure, even in the most recent aircrafts (Kermanidis, 2020). With the increasing use of adhesively bonded joints, understanding the characteristics of aluminum adherends has become highly relevant. Thus, this research aims to validate the design of an MMB apparatus for testing aluminum adherends numerically. The adhesive layer is modeled using cohesive zone model (CZM) and its mixed-mode behavior is modeled using Benzeggagh-Kenane (BK) model shown in Equation 1-1, which has been proven to yield satisfactory results (Salve & Jalwadi, 2015) (Benzeggagh & Kenane, 1996) in modeling the fracture of adhesive materials.

$$G_T = G_{IC} + (G_{IIC} - G_{IC}) \left(\frac{G_{II}}{G}\right)^{\eta} \tag{1.1}$$

2. APPARATUS DESIGN

The design of the MMB apparatus was made based on ASTM D6671 recommendation. Figure 21 shows the MMB apparatus base. This part is used to install roller supports that support the specimen.

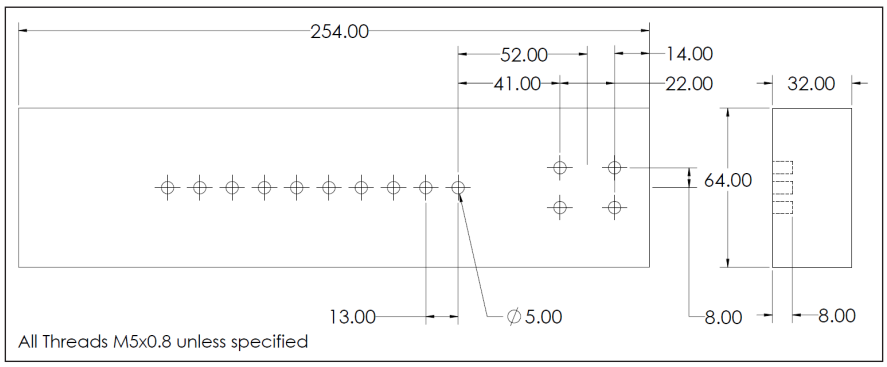

Figure 2-1: MMB Apparatus Base.

Figure 2-2 shows the MMB apparatus lever as the main part that delivers the mixed-mode loading to the specimen. The lever has screw holes on top to install the saddle and screw holes at the bottom to install roller supports and the hinge clamp.

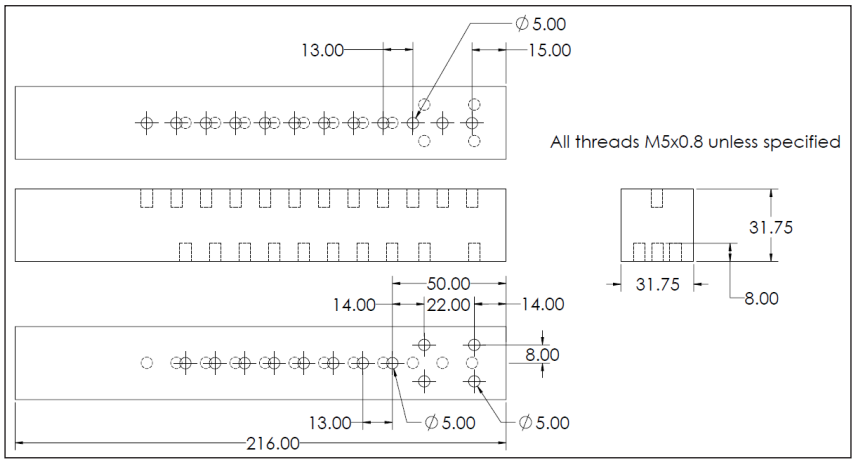

Figure 2-2: MMB Apparatus Lever.

Figure 2-3 shows the MMB apparatus hinge clamp. It is installed at the bottom of the lever and clamps the hinge and the tab that connects to the specimen. The hinge and tab designs are shown in Figure 2-4 and Figure 2-5, respectively.

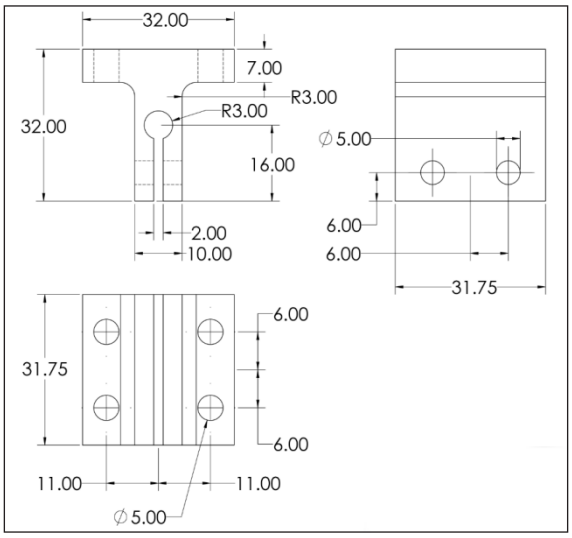

Figure 2-3: MMB Apparatus Hinge Clamp.

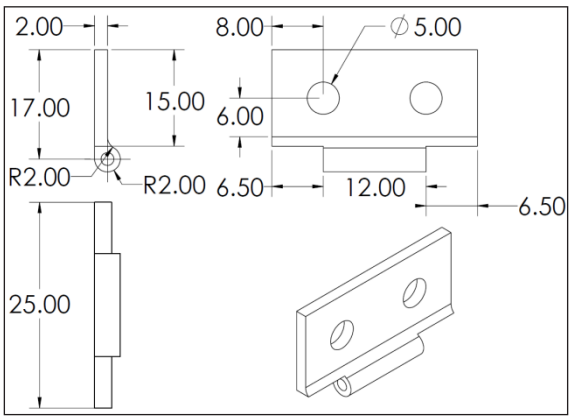

Figure 2-4: MMB Apparatus Hinge.

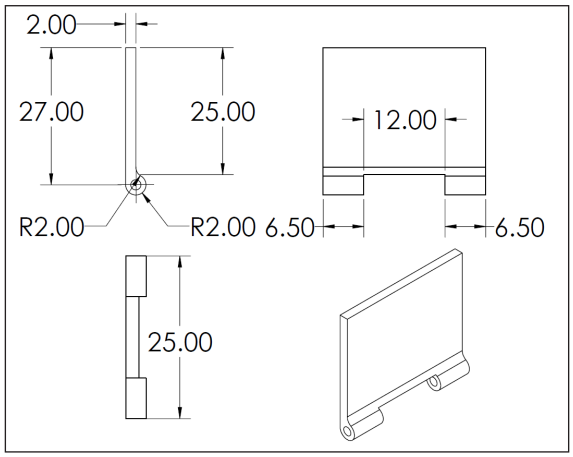

Figure 2.5: MMB Apparatus Tab.

Figure 2-6 shows the roller support, installed on the base to support the specimen and at the bottom of the lever to deliver loads onto the specimen. The roller uses standard R4A bearing, as recommended by ASTM D6671 to minimize friction.

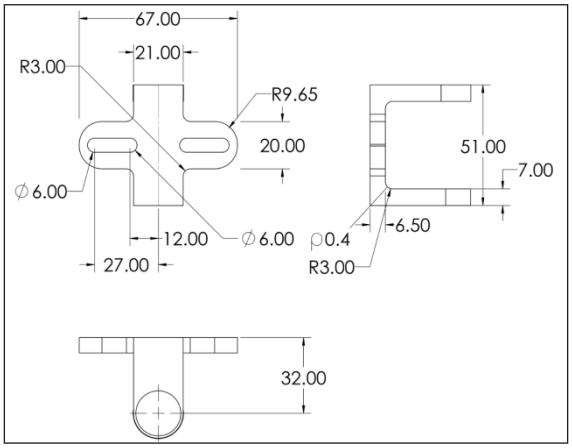

Figure 2.6: MMB Apparatus Roller Support.

The MMB apparatus uses a yoke-saddle configuration to apply the load from a general testing machine to the lever. Figure 2-7 shows the MMB apparatus saddle, which is installed on the lever. The saddle also uses standard R4A bearings.

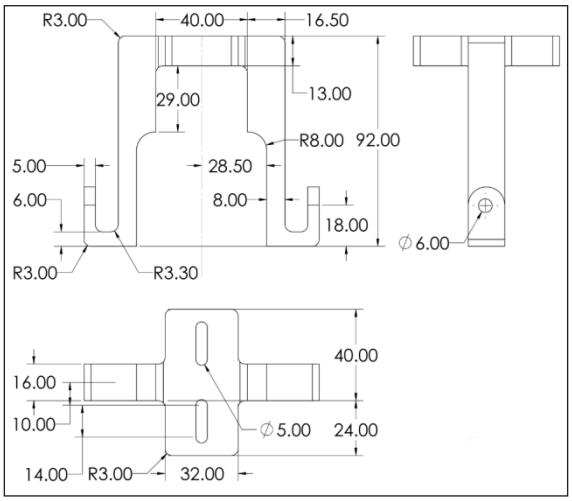

Figure 2-7: MMB Apparatus Saddle.

Figure 2-8 shows the yoke that delivers the load from a general testing machine to the saddle.

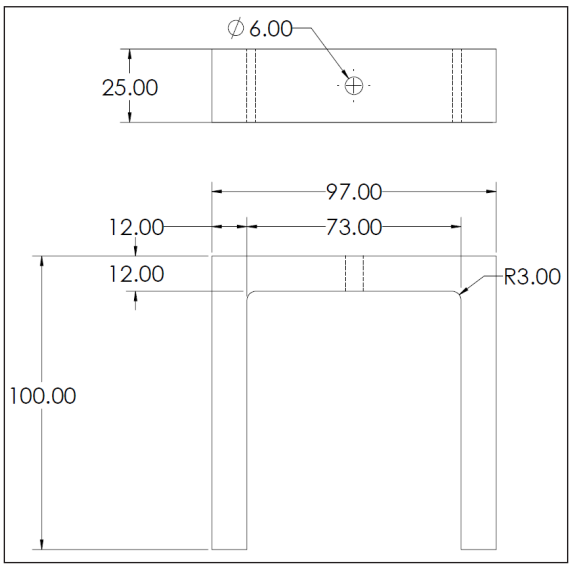

Figure 2-8: MMB Apparatus Yoke.

3. MODEL AND VARIATIONS

A simplified model of an MMB test was created. This simplified model omits the base and yoke-saddle installation of the MMB Apparatus design and replaces them as boundary conditions for simplicity.

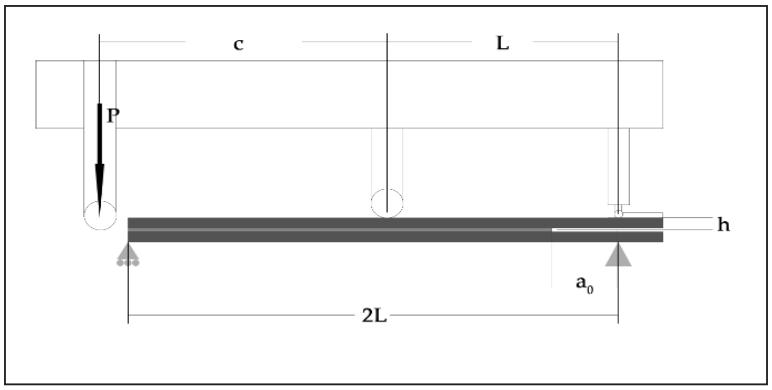

Figure 3-1: MMB Test Loading Setup and Dimensions.

Figure 3-1 shows the model and its loading setup. Table 31 tabulates the dimensions of the model and the specimen.

Table 3.1: Model Dimensions.

Dimension	Symbol	Value (mm)
Lever half-length		50
Loading arm	c	varied
Lever Width		31.75
Lever Thickness		31.75
Specimen Length	l	140
Specimen Half-Thickness	h	3.1
Specimen Initial Crack Length		25
Specimen Width		25

All specimen dimensions are chosen from the range stated in ASTM D6671. The base is modeled as a pin boundary condition. The yoke-saddle configuration is modeled as a rigid spring element in contact with the lever, as shown in Figure 3-2. The load is applied as prescribed displacement at the free end of the spring element.

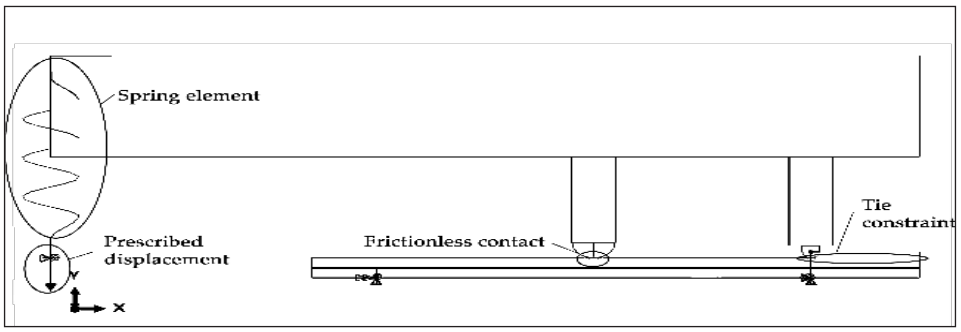

Figure 3-2: MMB Test Setup Model in ABAQUS.

The contact between the lever and the specimen and between the hinge and the tab is modeled as hard, frictionless contact. The tab is tied to the specimen. The materials used in this model are described in Table 3-2.

Table 3.2: Model Materials.

No	Material	Part
1	AA 6061	Apparatus (Lever, hinge, tab)
2	AA 6082 T651	Adherends
3	Araldite AV138	Adhesive layer

The properties of the materials used in this model are tabulated in Table 33.

Table 3.3: Material Properties.

Property	Value	Units
AA 6061		
Young's modulus	68900	MPa
Poisson's Ratio	0.3	
AA 6082 T651		
Young's modulus	70700	MPa
Poisson's Ratio	0.33	none
Araldite AV138		
Young's modulus	4890	MPa
Poisson's Ratio	0.35	none
Shear Modulus	1810	MPa
Tensile Strength	39.45	MPa
Shear Strength	30.2	MPa
G_{IC}	0.2	N/mm
G_{IIC}	0.38	N/mm

The use of aluminum 6061 for the apparatus refers to a commercial standard (Wyoming Test Fixtures, Inc., 2023) and is due to the material's availability in the region. The use of AA 6082 T651 and Araldite AV138 refers to Campilho's work (Viana, Campilho, & Rocha, 2019) Finite Element analysis based on ABAQUS software has been developed. The mesh size initially used in the numerical simulation is 0.2 mm, the same size as the thickness of the adhesive layer. Mesh convergence is then conducted for five element sizes: 1 mm, 0.75 mm, 0.5 mm, 0.2 mm, and 0.1 mm. The mesh convergence test is conducted for two cases: a mode-I dominant setup (GII/G = 0.166 with a loading arm length of 125 mm) and a pure mode-II setup (GII/G = 1 with a loading arm length of 17 mm).

Table 3.4: Simulation Setup Configuration.

Simulation	Loading arm (mm)	Estimated G_{II}/G
A	17.00	1.000
B	25.00	0.860
C	30	0.733
D	35	0.621
E	40	0.531
F	45.00	0.461
G	50	0.406
H	65.00	0.301

Simulation	Loading arm (mm)	Estimated G_{II}/G
I	85.00	0.229
J	105.00	0.190
K	125.00	0.166

The model uses continuum solid plane strain quadrilateral (CPE4) elements for the lever and the adherends, and cohesive two-dimensional quadrilateral (COH2D4) elements for the adhesive layer. The adhesive layer behavior is modeled using BK model with the power of 2. The simulation is run in set configurations of mixed-mode ratios tabulated in Table 3-4 to model the strength of the adhesive through a range of mixed-mode ratios.

To identify the validity and stability of the apparatus and understand its working range in testing aluminum adherends, a set of variations to the model is analyzed. The variations include adherend stiffness variations and adhesive G_{IC} input variations. The variations are described in Table 3-5. Regular simulation is the simulation with values directly referring to material properties used by Campilho [11].

Table 3-5: Model Variations.

Name	Variation
Regular Simulation	**-**
S1	Adherend Stiffness x0.5
S2	Adherend Stiffness x0.75
S3	Adherend Stiffness x1.25
S4	Adherend Stiffness x1.5
A1	Adhesive G_{IC} x0.5
A2	Adhesive G_{IC} x0.75
A3	Adhesive G_{IC} x1.25
A4	Adhesive G_{IC} x1.5
A5	Adhesive G_{IIC} x0.5
A6	Adhesive G_{IIC} x0.75
A7	Adhesive G_{IIC} x1.25
A8	Adhesive G_{IIC} x1.5

4. RESULTS AND ANALYSIS

G results from mesh convergence test were obtained and compared to values predicted by Equation (1-1) for the corresponding mixed-mode ratios. The calculated G value was 0.218 N/mm for the mode-I dominant setup (G_{II}/G = 0.166) and 0.380 for the pure mode-II setup. Figure 4-1 and Figure 4-2 show force vs. displacement graphs, Figure 4-3 and Figure 4-4 shows the model during the adhesive failure as an example, and Table 4-1 tabulates the errors with respect to the data in Table 3-3.

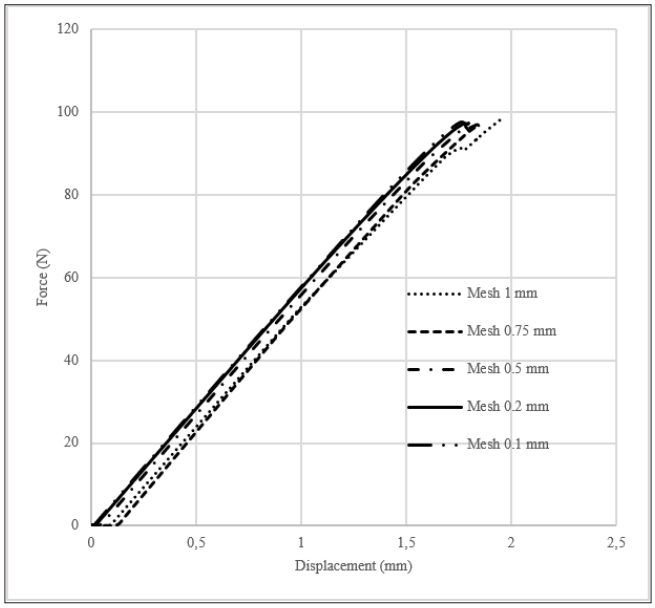

Figure 4-1: Force vs. Displacement Graph of G_I Dominant Mesh Convergence Check Results.

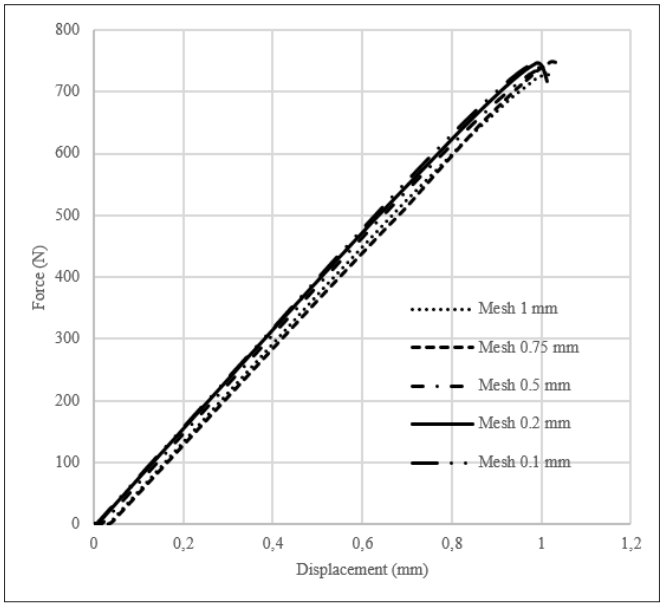

Figure 4-2: Force vs. Displacement Graph of G_{II} Dominant Mesh Convergence Check Results.

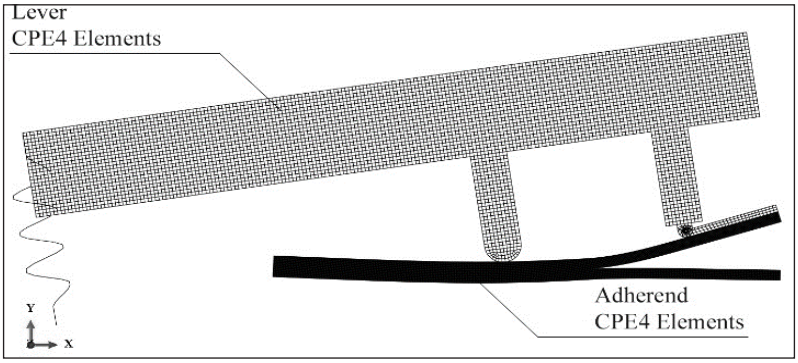

Figure 4-3: G_I Dominant Model Deformation (As an Example).

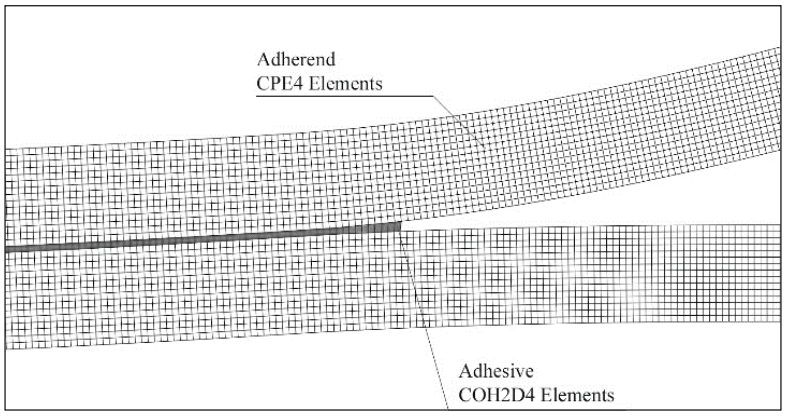

Figure 4-4: G_I Dominant Model Deformation, Zoomed in (Example).

Table 4-1 shows that mode-I dominant simulation yields results with errors below 5% at mesh sizes 0.75 mm or smaller. Mesh size 0.5 mm gives the smallest error, but the result converges (stabilizes) at mesh sizes 0.2 mm or lower. Pure mode-II simulation yields convergent results at mesh sizes 0.5 or lower. Thus, the simulations use a mesh size of 0.2 mm for further variations to obtain sufficiently accurate results while maintaining an optimal computational load. Figure 4-5 shows the G_I and G_{II} mapping of the regular simulation. Figure 4-6 shows the maximum displacement at peak force for the chosen mixed-mode ratios in Table 3-4.

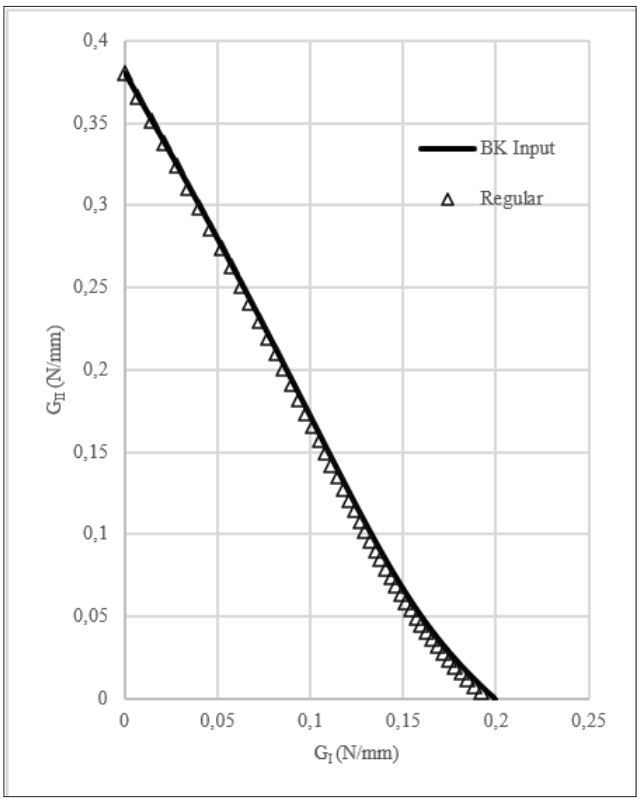

Figure 4-5: G_I / G_{II} Chart of Regular Simulation Result.

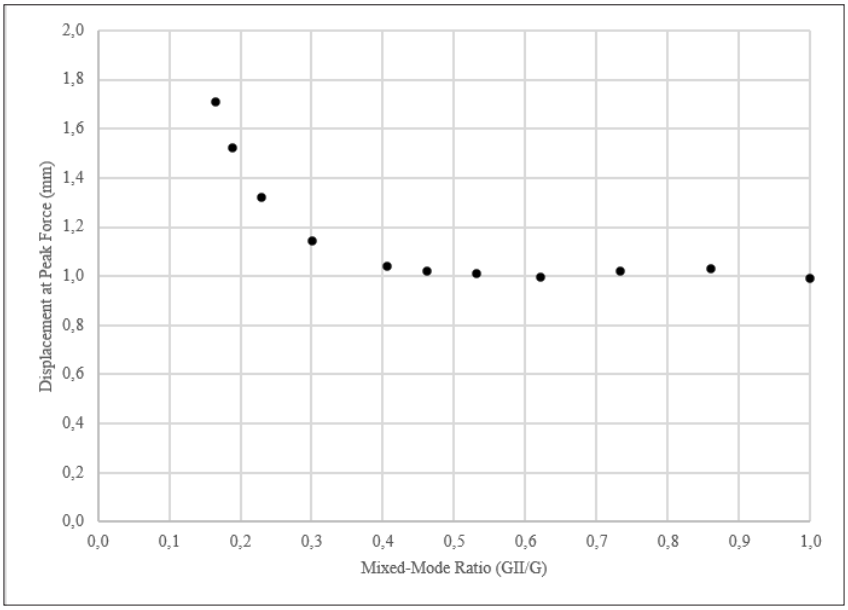

Figure 4-6: Displacement at Peak Force vs. Mixed-Mode Ratio Chart of Regular Simulation Result.

ASTM D6671 includes a criterion for minimizing errors due to geometrical nonlinearity as shown in Equation 4-1.

$$\delta^{max} = L\left[0.27 - 0.06\left(\frac{G_{II}}{G}\right)\right] \quad (4\text{-}1)$$

When this criterion is fulfilled, errors due to geometrical nonlinearity should not exceed 5%. Using L = 50 cm, we would obtain that the maximum allowed displacement for any mixed-mode ratio is greater than 10 cm. The results shown in Figure 4-6 thus confirm that the chosen specimen is in the MMB apparatus design's work range. This aspect is also inspected for stiffness variations, and G_{IC} variations to further check the validity of the design and test aluminum adherends.

Table 4-1: Mesh Convergence Result and Errors.

Mesh Size **(mm)**	Mode-I dominant **G result (N/mm)**	Error (%)	Pure mode-II **G result (N/mm)**	Error (%)
1	0.195	-10.36	0.400	5.27
0.75	0.216	-0.82	0.389	2.42
0.5	0.213	-2.11	0.376	-1.10
0.2	0.210	-3.53	0.376	-1.15
0.1	0.209	-3.92	0.378	-0.55

The results of stiffness variations are tabulated in Table 43 and mapped in Figure 4-7. Differences in accuracy are visible in each variation. The G_{IC} error, G_{IIC} error, and the root mean squared (RMS) error of the regression are also shown in Figure 4-8. Displacement at peak force for each variation is also shown in Figure 4-9.

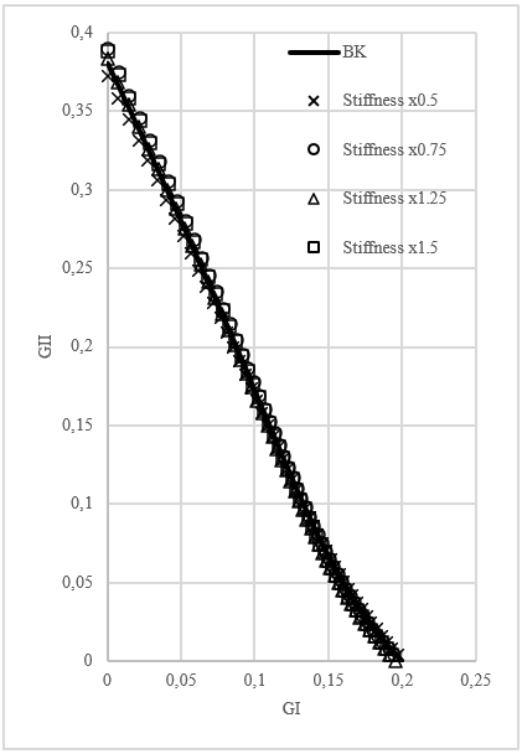

Figure 4-7: G_I/G_{II} Chart of Stiffness Variation Results.

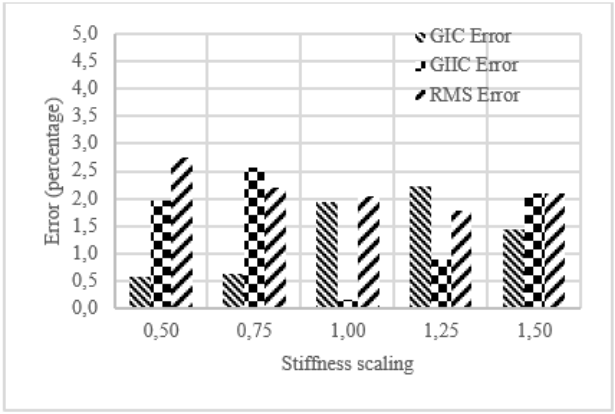

Figure 4-8: Error Charts of Stiffness Variation Results.

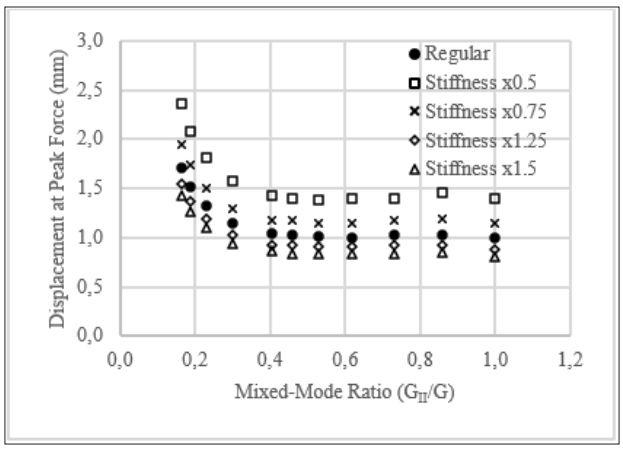

Figure 4-9: Displacement at Peak Force vs. Mixed-Mode Ratio Chart of Stiffness Variation Results.

Errors of G_{IC} and G_{IIC} fluctuate visibly, but the MSE of the whole regression is relatively stable, with a tendency to decrease by increasing adherend stiffness. Displacements that occur are below the maximum allowed displacement in Equation (4-1). In agreement, errors in all results of stiffness variation do not exceed 3%. It is evident that the displacements that occur increase as the stiffness decreases, but the pattern throughout the mixed-mode ratios remains unchanged. It can be concluded that the design is valid for testing aluminum adherends with various stiffness levels, with a tendency to perform better for stiffer adherends. The results of GIC input variations are tabulated in Table 4-4. Differences in accuracy are also visible in each variation. The G_{IC} error, G_{IIC} error, and the RMS error of the regression are also shown in Figure 4-10. Displacement at peak force for each variation is also shown in Figure 4-11.

Table 4-3: Stiffness Variation Results and Errors.

Variation	Stiffness Input (MPa)	G_{IC} (N/mm)	G_{IC} Error (%)	G_{IIC} (N/mm)	G_{IIC} Error (%)	RMS Error (%)
Regular	70700	0.201	0.57	0.373	1.96	2.75
Adherend Stiffness x0.5	35350	0.201	0.57	0.373	1.96	2.75
Adherend Stiffness x0.75	53025	0.199	0.63	0.390	2.57	2.20
Adherend Stiffness x1.25	88375	0.196	2.23	0.383	0.90	1.79
Adherend Stiffness x1.5	106050	0.197	1.44	0.388	2.11	2.09

Note: G_I and G_{II} errors are calculated with respect to the input (G_I = 0.213 N/mm and G_{II} = 0.38 N/mm)

Table 4-4: Adhesive G_{IC} Strength Variation Results and Errors.

Variation	G_{IC} Input (N/mm)	G_{IC} (N/mm)	G_{IC} Error (%)	G_{IIC} (N/mm)	G_{IIC} Error (%)	RMS Error (%)
Regular	0.2	0.196	1.95	0.381	0.17	2.03
Adhesive G_{IC} x0.5	0.1	0.098	2.17	0.381	0.26	1.61
Adhesive G_{IC} x0.75	0.15	0.147	2.12	0.384	1.00	2.18
Adhesive G_{IC} x1.25	0.25	0.248	0.91	0.385	1.39	2.48
Adhesive G_{IC} x1.5	0.3	0.300	0.12	0.377	0.91	2.30

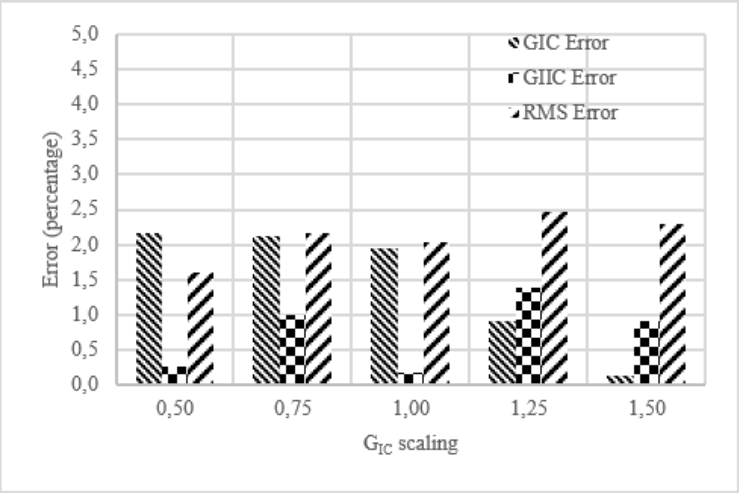

Figure 4-10: Error Charts of Adhesive G_{IC} Strength Variation Results.

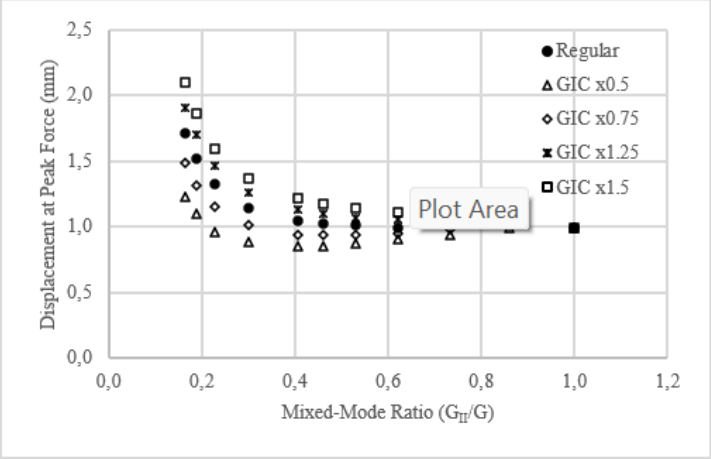

Figure 4-11 Displacement at Peak Force vs Mixed-Mode Ratio Chart of Adhesive G_{IC} Strength Variation Results.

G_{IC}, G_{IIC}, and RMS errors seem to get higher with increasing G_{IC}. Displacements that occur are below the maximum allowed displacement in Equation (1-1). In agreement, errors in all results of G_{IC} variation do not exceed 3%, which indicates the design's validity. It can be seen that by increasing G_{IC}, displacement that occurs on lower mixed-mode ratios (near pure mode I) also increases. It can be concluded that the design is valid, with a tendency to perform better in testing weaker adhesives. The result of G_{IIC} variations is tabulated in Table 45. Differences in accuracy are visible in each variation. The G_{IC} error, G_{IIC} error, and the root mean squared (RMS) error of the regression are also shown in Figure 4-12. Displacement at peak force for each variation is also shown in Figure 4-13.

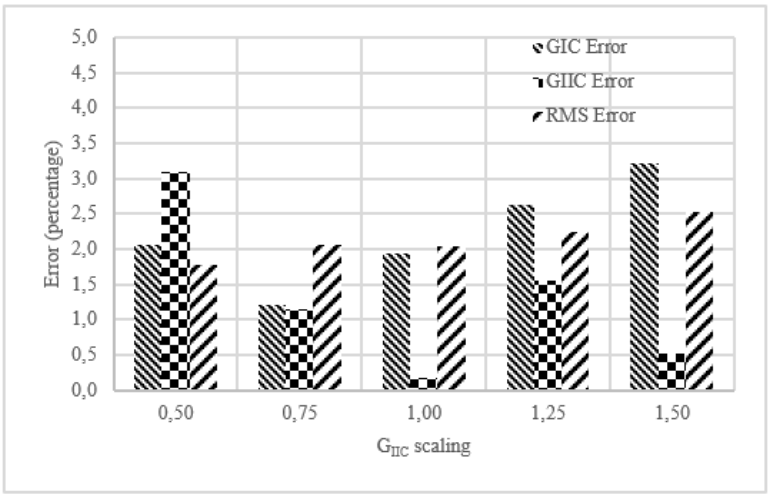

Figure 4-12: Error Charts of Adhesive G_{IIC} Strength Variation Results.

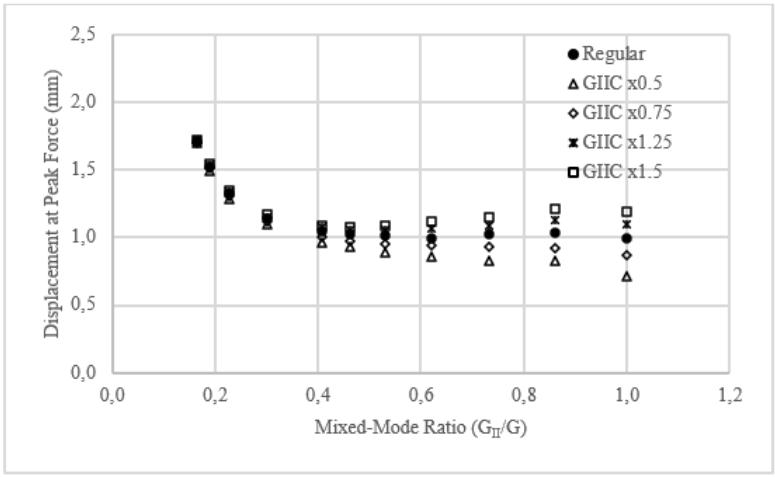

Figure 4-13: Displacement at Peak Force vs Mixed-Mode Ratio Chart of Adhesive G_{IIC} Strength Variation Results.

Table 4-5: Adhesive G_{IIC} Strength Variation Results and Errors.

Variation	G_{IIC} Input (N/mm)	G_{IC} (N/mm)	G_{IC} Error (%)	G_{IIC} (N/mm)	G_{IIC} Error (%)	RMS Error (%)
Regular	0.38	0.196	1.95	0.381	0.166	2.03
Adhesive G_{IC} x0.5	0.19	0.196	2.07	0.196	3.089	1.77
Adhesive G_{IC} x0.75	0.285	0.198	1.21	0.282	1.157	2.06
Adhesive G_{IC} x1.25	0.475	0.195	2.62	0.468	1.546	2.25
Adhesive G_{IC} x1.5	0.57	0.194	3.22	0.573	0.520	2.52

G_{IC} and G_{IIC} errors fluctuate visibly, but RMS errors steadily get higher with increasing G_{IIC}. Displacements that occur are below the maximum allowed displacement in Equation 1-1. In agreement, errors in all results of G_{IC} variation do not exceed 4%, which indicates the design's validity. It can be seen that by increasing G_{IIC}, the displacement that occurs on higher mixed-mode ratios (near pure mode-II) also increases. It can be concluded that the design is valid, with a tendency to perform better in testing weaker adhesives.

5. CONCLUSION

As understanding adhesive joint strength under mixed-mode loadings becomes increasingly relevant, a design of MMB apparatus has been developed based on ASTM D6671 recommendations for testing aluminium adherends. A finite element model has been made in ABAQUS to validate the design. Mesh convergence test yields convergence for mesh sizes 0.2 mm or lower. The model has successfully mapped the mixed-mode behavior of adhesive material through a set of MMB tests on aluminum adherends with sufficient accuracy. Thus, the proposed design of MMB Apparatus is deemed valid for testing aluminum adherends, with a tendency to perform better in testing stiffer aluminum adherends or weaker adhesives.

ACKNOWLEDGEMENT

The presented work is funded by Institut Teknologi Bandung Through P2MI 2024.

REFERENCES

American Society for Testing and Materials. (2006). Standard Test Method for Mixed Mode I-Mode II Interlaminar Fracture Toughness of Unidirectional Fiber Reinforced Polymer Matrix Composites. West Conshohocken: ASTM International.

Benzeggagh, M. L., & Kenane, M. (1996). Measurement of mixed mode delamination fracture toughness of unidirectional glass/epoxy composites with mixed-mode bending apparatus. *Composite Science and Technology* (56), 439-449.

Borges, C. S., Akhavan-Safar, A., Tsokanas, P., Carbas, R. J., Marques, E. A., & da Silva, L. F. (2023). From fundamental concepts to recent developments in the adhesive bonding technology: a general view. *Discover Mechanical Engineering, 2*(8).

Kermanidis, A. T. (2020). Revolutionizing Aircraft Materials and Processes. In *Aircraft Alumunium Alloys: Application and Future Trends.* Springer Link.

Marques, A. C., Mocanu, A., Tomi´c, N. Z., Balos, S., Stammen, E., Lundevall, A., . . . de Freitas, S. T. (2020). Review on Adhesives and Surface Treatments for Structural Applications: Recent Developments on Sustainability and Implementation for Metal and Composite Substrates. *Materials MDPI, 13*(5590).

Reeder, J. R. (2003). A Criterion to Control Nonlinear Error in the Mixed-Mode Bending Test. *Composite Material: Testing and Design, 14*.

Reeder, J. R., & Crews, J. H. (1988). A MIXED-MODE BENDING APPARATUS FOR DELAMINATION TESTING. *NASA TECHNICAL MEMORANDUM*(1000662).

Reeder, J. R., & Crews, Jr., J. H. (1991). NONLINEAR ANALYSIS AND REDESIGN OF THE MIXED-MODE BENDING DELAMINATION TEST. *NASA TECHNICAL MEMORANDUM*(102777).

Salve, A., & Jalwadi, S. N. (2015). Implementation of Cohesive Zone in ABAQUS to Investigate Fracture Problems. *National Conference for Engineering Post Graduates RIT.*

Viana, F., Campilho, R. D., & Rocha, R. J. (2019). Fracture modelling of adhesively-bonded joints by an inverse method. *Frattura ed Integrità Strutturale, 48*.

Wyoming Test Fixtures, Inc. (2023). *Wyoming Test Fixtures*. (Wyoming Test Fixtures, Inc.) Retrieved 12 21, 2023, from https://wyomingtestfixtures.com/products/fracture-toughness/mixed-mode-bending-fracture-toughness-test-fixture-astm-d-6671/